Appl. Math. Mech. -Engl. Ed., **42**(8), 1155–1170 (2021)

APPLIED MATHEMATICS AND MECHANICS (ENGLISH EDITION)

https://doi.org/10.1007/s10483-021-2760-8

Radial integral boundary element method for simulating phase change problem with mushy zone*

Hongxiao YAO[1,2], Weian YAO[1,2,†], Chong ZUO[3], Xiaofei HU[1,2]

1. State Key Laboratory of Structural Analysis for Industrial Equipment, Dalian University of Technology, Dalian 116024, Liaoning Province, China;
2. International Center for Computational Mechanics, Dalian University of Technology, Dalian 116024, Liaoning Province, China;
3. Sany Heavy Industry Co. Ltd., Wuhan 430100, China

(Received Mar. 24, 2021 / Revised Jun. 12, 2021)

Abstract A radial integral boundary element method (BEM) is used to simulate the phase change problem with a mushy zone in this paper. Three phases, including the solid phase, the liquid phase, and the mushy zone, are considered in the phase change problem. First, according to the continuity conditions of temperature and its gradient on the liquid-mushy interface, the mushy zone and the liquid phase in the simulation can be considered as a whole part, namely, the non-solid phase, and the change of latent heat is approximated by heat source which is dependent on temperature. Then, the precise integration BEM is used to obtain the differential equations in the solid phase zone and the non-solid phase zone, respectively. Moreover, an iterative predictor-corrector precise integration method (PIM) is needed to solve the differential equations and obtain the temperature field and the heat flux on the boundary. According to an energy balance equation and the velocity of the interface between the solid phase and the mushy zone, the front-tracking method is used to track the move of the interface. The interface between the liquid phase and the mushy zone is obtained by interpolation of the temperature field. Finally, four numerical examples are provided to assess the performance of the proposed numerical method.

Key words phase change, mushy zone, boundary element method (BEM), precise integration method (PIM)

Chinese Library Classification O241.4, O414.13
2010 Mathematics Subject Classification 65M38, 80A22

1 Introduction

For pure media, the phase change takes place at the unique temperature, two phases including the solid phase and the liquid phase and one interface between these two phases

* Citation: YAO, H. X., YAO, W. A., ZUO, C., and HU, X. F. Radial integral boundary element method for simulating phase change problem with mushy zone. *Applied Mathematics and Mechanics* (*English Edition*), **42**(8), 1155–1170 (2021) https://doi.org/10.1007/s10483-021-2760-8

† Corresponding author, E-mail: ywa@dlut.edu.cn

Project supported by the National Natural Science Foundation of China (No. 11672064)

need to be considered. However, for mixed media such as alloys, phase change takes place in a range of temperature. Therefore, there are three phases and two interfaces to be considered, which are the solid phase, the liquid phase, and the mushy zone. In the mushy zone, some parts of the media have changed their phases, while the other parts have not. That is to say, both solid and liquid are mixed in the mushy zone[1].

For phase change problems, it is vital to handle the moving interface between phases and the releasing or absorbing of latent heat[2], and the fixed-domain method and the front-tracking method are commonly-used methods. For the fixed-domain method, all the phase change domains, including the solid phase, the liquid phase, and the mushy zone, are considered as a continuous medium as a whole part[3]. The changes of latent heat are described implicitly in the uniform nonlinear heat conduction equations where enthalpy, effective heat capacity, and heat source terms are involved[4–5]. For the fixed-domain method, it is easier to program, but the nonlinear equations need to be solved, and the phase change interface needs to be obtained by interpolation of temperatures. If the latent heat or the temperature variation is large, or there is discontinuity or even a big step-jump of enthalpy, it would be difficult to reach the convergence. The front-tracking method, which needs the moving mesh of the grid, solves heat conduction problems separately in different phases, and tracks the moving interface based on the interface energy condition[6]. Therefore, the front-tracking method is more suitable for phase change problems with large discontinuity or a step-jump of enthalpy than the fixed-domain method.

The numerical methods, including the finite difference method, the finite element method (FEM), the finite volume method, the meshless method, and the boundary element method (BEM)[7–8], are the mainly used space-discretization methods. The extended FEM is one of the favourite approaches to deal with problems with discontinuity and moving boundaries by using nodal extended shape functions and additional nodal degrees of freedom[9], which has been used in phase change problems[10–11] and incompressible two-phase flow problems[12]. The BEM has been reported to be one of the favourite tools for a wide variety of heat conduction problems[13–15]. Because the moving or unknown boundary can be easily discretized by boundary elements, compared with other numerical methods, it is very convenient to apply the BEM for grid deforming problems, such as moving boundary problems and geometrical inverse problems[16]. For example, the BEM and the front-tracking method are used to solve the phase change problem during a continuous pure medium casting process[17]. The BEM and the level set method are used to deal with the complicated topological change of an interface during phase change[18]. The BEM is applied in a direct inversion scheme to identify the shape of cavity[19]. Compared with other methods, the main advantage of the BEM is that only the boundary needs to be discretized into elements, and internal nodes can be distributed freely according to actual demand. Once the velocity and direction of the moving boundary are determined, the new location of moving boundary nodes can be obtained very easily, and then the new boundary elements are formed automatically. During the re-meshing process, boundary nodes and internal nodes can be added or deleted if needed.

When the BEM is applied, to circumvent the domain discretization in the derived integral equation, the domain integrals need to be transformed into boundary integrals. The radial integral method (RIM) is one of the commonly-used transforming approaches. It is based on pure mathematical treatments, and could transform any kind of domain integrals into boundary integrals without using the Laplace operator and particular solutions of the problem[20–22]. To solve the time-dependent differential equations generated by the BEM, the precise integration method (PIM) is a good choice because of its high accuracy and unconditional stability[23–24].

This paper is intended to combine the radial integral BEM with the front-tracking method to solve the phase change problem with a mushy zone. In the mushy zone, the changes of latent heat are approximated into heat source terms, and then the mushy zone and the liquid domain are treated as a whole part. The integral equation for nonlinear heat conduction with source is derived based on the fundamental solution of Laplace equation. Then, the RIM[20] is used

to transform the arising domain integrals into boundary integrals. In the time domain, the PIM[23] is used to solve nonlinear differential equations, and then the heat fluxes on the moving boundary are obtained. Based on the energy balance equation on the moving boundary, the velocity can be obtained. The front-tracking method is used to track the move of the interface between the solid phase and the mushy zone. However, the interface between the liquid phase and the mushy zone is obtained by interpolation of the temperature field.

2 Governing equations of phase change problem with mushy zone

A two-dimensional domain Ω_{total} is considered, where the phase change with the mushy zone takes place. Contrary to the isothermal phase change problems, the interval of phase change temperature is $(T_{\text{ms}}, T_{\text{ml}})$. Therefore, the domain Ω_{total} is divided into three regions, namely solid domain Ω_{s}, mushy zone Ω_{m}, and liquid domain Ω_{l}, by two interfaces Γ_{ms} and Γ_{ml}, as shown in Fig. 1. If volumetric changes are neglected and the density is constant, the heat conduction governing differential equations can be written as

$$\nabla \cdot (k_{\text{s}} \nabla T_{\text{s}}(\boldsymbol{x}, t)) + Q_{\text{s}}(\boldsymbol{x}, t) = \rho c_{\text{s}} \frac{\partial T_{\text{s}}(\boldsymbol{x}, t)}{\partial t}, \quad \boldsymbol{x} \in \Omega_{\text{s}}, \tag{1}$$

$$\nabla \cdot (k_{\text{m}} \nabla T_{\text{m}}(\boldsymbol{x}, t)) + Q_{\text{m}}(\boldsymbol{x}, t) + \rho L \frac{\mathrm{d}f}{\mathrm{d}t} = \rho c_{\text{m}} \frac{\partial T_{\text{m}}(\boldsymbol{x}, t)}{\partial t}, \quad \boldsymbol{x} \in \Omega_{\text{m}}, \tag{2}$$

$$\nabla \cdot (k_{\text{l}} \nabla T_{\text{l}}(\boldsymbol{x}, t)) + Q_{\text{l}}(\boldsymbol{x}, t) = \rho c_{\text{l}} \frac{\partial T_{\text{l}}(\boldsymbol{x}, t)}{\partial t}, \quad \boldsymbol{x} \in \Omega_{\text{l}}, \tag{3}$$

where $\boldsymbol{x} = (x_1, x_2)$, $\nabla = \frac{\partial(\cdot)}{\partial x_1}\boldsymbol{i} + \frac{\partial(\cdot)}{\partial x_2}\boldsymbol{j}$, T denotes the temperature, t is the time, ρ is the density, and Q denotes the heat source. c represents the heat capacity, and k is the thermal conductivity. The subscripts 's', 'l', and 'm', respectively, denote the solid domain, the liquid domain, and the mushy zone. The heat capacities and thermal conductivities may be non-constant in these three domains, but in Ω_{total}, they are continuous functions with respect to the temperature.

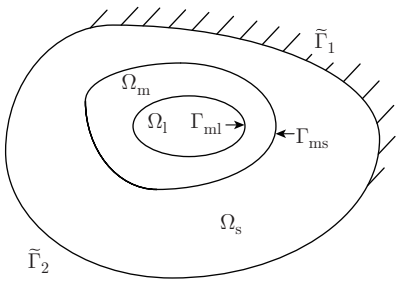

Fig. 1 Schematic diagram of phase change problem

The phase change latent heat is in Eq. (2) of the mushy zone L, and f is the solid phase fraction. It is assumed that f equals 0 on Γ_{ml}, f equals f_{su} on Γ_{ms}, and f is a function with respect to temperature or distance to the interfaces Γ_{ms} and Γ_{ml}[25].

The boundary conditions of Ω_{total} are given by

$$T(\boldsymbol{x}, t) = \overline{T}(\boldsymbol{x}, t), \quad \boldsymbol{x} \in \widetilde{\Gamma}_1, \tag{4}$$

$$q(\boldsymbol{x}, t) \equiv -k \frac{\partial T(\boldsymbol{x}, t)}{\partial \boldsymbol{n}} = \overline{q}(\boldsymbol{x}, t), \quad \boldsymbol{x} \in \widetilde{\Gamma}_2, \tag{5}$$

where $\boldsymbol{n}$ denotes the unit outside normal vector, and q is the heat flux.

The initial condition is given by

$$T(\boldsymbol{x}, 0) = T_0(\boldsymbol{x}), \quad t = 0. \tag{6}$$

Besides, there are interface conditions on the interfaces $\Gamma_{\rm ms}$ and $\Gamma_{\rm ml}$. The temperature conditions and the energy equation on the solid-mushy interface $\Gamma_{\rm ms}$ are given by

$$T(\boldsymbol{x},t)=T_{\rm ms},\quad \boldsymbol{x}\in\Gamma_{\rm ms}, \tag{7}$$

$$k_{\rm s}\frac{\partial T_{\rm s}(\boldsymbol{x},t)}{\partial \boldsymbol{n}_{\rm s}}-k_{\rm m}\frac{\partial T_{\rm m}(\boldsymbol{x},t)}{\partial \boldsymbol{n}_{\rm s}}=\rho L(1-f_{\rm su})V_{\rm n},\quad \boldsymbol{x}\in\Gamma_{\rm ms}, \tag{8}$$

where $V_{\rm n}$ is the velocity of the moving interface. The temperature conditions and the energy equation on the liquid-mushy interface $\Gamma_{\rm ml}$ are given by

$$T(\boldsymbol{x},t)=T_{\rm ml},\quad \boldsymbol{x}\in\Gamma_{\rm ml}, \tag{9}$$

$$k_{\rm l}\frac{\partial T_{\rm l}(\boldsymbol{x},t)}{\partial \boldsymbol{n}_{\rm l}}=k_{\rm m}\frac{\partial T_{\rm m}(\boldsymbol{x},t)}{\partial \boldsymbol{n}_{\rm l}},\quad \boldsymbol{x}\in\Gamma_{\rm ml}. \tag{10}$$

It can be found that from Eqs. (7) and (9), the temperature is continuous. Since the thermal conductivities are continuous in the whole domain, it can also be found from Eqs. (8) and (10) that the temperature gradient is continuous on $\Gamma_{\rm ml}$ but stepped on $\Gamma_{\rm ms}$. However, if the latent heat change in the mushy zone is treated as the source terms, the mushy zone and the liquid phase in the simulation are treated as a whole part, namely the non-solid phase, and let $\Omega_{\rm ns}=\Omega_{\rm m}\cup\Omega_{\rm l}$. Then, the differential equation in the non-solid domain is written as follows:

$$\nabla\cdot(k(T)\nabla T(\boldsymbol{x},t))+Q_{\rm ns}(\boldsymbol{x},t,T)=\rho c(T)\frac{\partial T(\boldsymbol{x},t)}{\partial t},\quad \boldsymbol{x}\in\Omega_{\rm ns}, \tag{11}$$

where

$$Q_{\rm ns}(\boldsymbol{x},t,T)=\begin{cases}Q_{\rm m}(\boldsymbol{x},t)+\rho L\dfrac{{\rm d}f}{{\rm d}t}, & \boldsymbol{x}\in\Omega_{\rm m},\\ Q_{\rm l}(\boldsymbol{x},t), & \boldsymbol{x}\in\Omega_{\rm l}.\end{cases} \tag{12}$$

Therefore, the phase change problem can be dealt with by separating the whole domain into two parts, namely the solid domain and the non-solid domain. Not only Eq. (1) of solid domain, Eq. (11) of non-solid domain, and the solid-mushy interface conditions (see Eqs. (7) and (8)), but also the whole domain's boundary conditions (see Eqs. (4) and (5)) and the initial condition (see Eq. (6)) need to be solved. First, the transient heat conduction problems are solved by the precise integration BEM. Then, the moving velocity of the mushy-solid interface $\Gamma_{\rm ms}$ can be obtained by Eq. (8), and the moving position of $\Gamma_{\rm ms}$ can be tracked by an iteration procedure of the front-tracking method. Finally, the mushy-liquid interface $\Gamma_{\rm ml}$ can be obtained by interpolation of temperature field.

3 Implementation of precise integration BEM

The transient heat conduction problems in the solid domain and the non-solid domain are solved by the precise integration BEM, respectively. The governing equation in the solid domain or non-solid domain can be rewritten in a uniform equation as follows:

$$\nabla\cdot(k(T)\nabla T(\boldsymbol{x},t))+Q(\boldsymbol{x},t,T)=\rho c(T)\frac{\partial T(\boldsymbol{x},t)}{\partial t}. \tag{13}$$

According to the whole domain's boundary conditions (see Eqs. (4) and (5)) and the solid-mushy interface condition (see Eq. (7)), the boundary conditions for the solid domain or the non-solid domain can be rewritten as follows:

$$T(\boldsymbol{x},t)=\overline{T}(\boldsymbol{x},t),\quad \boldsymbol{x}\in\Gamma_1, \tag{14}$$

$$q(\boldsymbol{x},t)\equiv-k\frac{\partial T(\boldsymbol{x},t)}{\partial \boldsymbol{n}}=\overline{q}(\boldsymbol{x},t),\quad \boldsymbol{x}\in\Gamma_2. \tag{15}$$

The Green function $G(\boldsymbol{x},\boldsymbol{y})$ is adopted as the weight function to derive the boundary-domain integral equation. For two-dimensional problems, it is expressed as

$$G(\boldsymbol{x},\boldsymbol{y})=\frac{1}{2\pi}\ln\frac{1}{r(\boldsymbol{x},\boldsymbol{y})},\quad r(\boldsymbol{x},\boldsymbol{y})=\|\boldsymbol{x}-\boldsymbol{y}\|_2\,. \tag{16}$$

Both sides of Eq. (13) are multiplied by G. Then, the resulting equation is integrated over the domain Ω. Applying the integration by parts and using Gauss' divergence theorem, one can get

$$\begin{aligned}c(\boldsymbol{y})k(T)T(\boldsymbol{y},t)=&\int_\Gamma G(\boldsymbol{x},\boldsymbol{y})k(T)\frac{\partial T(\boldsymbol{x},t)}{\partial x_i}n_i\mathrm{d}\Gamma-\int_\Gamma k(T)T(\boldsymbol{x},t)\frac{\partial G(\boldsymbol{x},\boldsymbol{y})}{\partial x_i}n_i\mathrm{d}\Gamma\\&+\int_\Omega T(\boldsymbol{x},t)\frac{\partial k(T)}{\partial x_i}\frac{\partial G(\boldsymbol{x},\boldsymbol{y})}{\partial x_i}\mathrm{d}\Omega-\int_\Omega G(\boldsymbol{x},\boldsymbol{y})Q(\boldsymbol{x},t,T)\mathrm{d}\Omega\\&-\rho\int_\Omega G(\boldsymbol{x},\boldsymbol{y})c(T)\frac{\partial T(\boldsymbol{x},t)}{\partial t}\mathrm{d}\Omega,\end{aligned} \tag{17}$$

where $c(\boldsymbol{y})=1$ when $\boldsymbol{y}\in\Omega$, and $c(\boldsymbol{y})=\varphi(\boldsymbol{y})/(2\pi)$ when $\boldsymbol{y}\in\Gamma$, in which φ denotes the interior angle in radians.

Equation (17) can be rewritten as[26]

$$\begin{aligned}c(\boldsymbol{y})\widetilde{T}(\boldsymbol{y},t)=&\int_\Gamma G(\boldsymbol{x},\boldsymbol{y})\frac{\partial\widetilde{T}(\boldsymbol{x},t)}{\partial x_i}n_i\mathrm{d}\Gamma-\int_\Gamma\widetilde{T}(\boldsymbol{x},t)\frac{\partial G(\boldsymbol{x},\boldsymbol{y})}{\partial x_i}n_i\mathrm{d}\Gamma\\&+\int_\Omega\widetilde{T}(\boldsymbol{x},t)v(\boldsymbol{x},\boldsymbol{y},T)\mathrm{d}\Omega-\int_\Omega G(\boldsymbol{x},\boldsymbol{y})Q(\boldsymbol{x},t,T)\mathrm{d}\Omega\\&-\rho\int_\Omega G(\boldsymbol{x},\boldsymbol{y})\frac{c(T)}{k(T)}\frac{\partial\widetilde{T}(\boldsymbol{x},t)}{\partial t}\mathrm{d}\Omega,\end{aligned} \tag{18}$$

where

$$\widetilde{T}(\boldsymbol{x},t)=k(T)T(\boldsymbol{x},t), \tag{19a}$$

$$v(\boldsymbol{x},\boldsymbol{y},T)=\frac{\partial\widetilde{k}(T)}{\partial T}\frac{\partial T}{\partial x_i}\frac{\partial G(\boldsymbol{x},\boldsymbol{y})}{\partial x_i}, \tag{19b}$$

$$\widetilde{k}(T)=\ln k(T). \tag{19c}$$

In Eq. (18), the domain integral, where the source function $Q(\boldsymbol{x},t,T)$ is involved, can be directly transformed by the RIM[20] as follows:

$$\int_\Omega G(\boldsymbol{x},\boldsymbol{y})f(\boldsymbol{x},t)\mathrm{d}\Omega(\boldsymbol{x})=\int_\Gamma\frac{F(\boldsymbol{z},\boldsymbol{y})}{r(\boldsymbol{z},\boldsymbol{y})}\frac{\partial r}{\partial\boldsymbol{n}}\mathrm{d}\Gamma, \tag{20}$$

where

$$F(\boldsymbol{z},\boldsymbol{y})=\int_0^{r(\boldsymbol{z},\boldsymbol{y})}G(\boldsymbol{x},\boldsymbol{y})Q(\boldsymbol{x},t,T)\xi\mathrm{d}\xi. \tag{21}$$

In order to transform the third domain integral in Eq. (18), the following approximation needs to be done:

$$\frac{c(T)}{k(T)}\frac{\partial\widetilde{T}(\boldsymbol{x},t)}{\partial t}=\sum_{i=1}^{N}\alpha_i\phi_i(R)+\overline{\alpha}_1x_1+\overline{\alpha}_2x_2+\overline{\alpha}_3, \tag{22}$$

where $R=\|\boldsymbol{x}-\boldsymbol{x}_i\|$, $\phi_i(R)$ is the radial basis function (RBF), and α_i and $\overline{\alpha}_i$ are coefficients.

According to Ref. [27], the transformation is done as follows:

$$\int_{\Omega} G(\boldsymbol{x},\boldsymbol{y})\frac{c(T)}{k(T)}\frac{\partial\widetilde{T}(\boldsymbol{x},t)}{\partial t}\mathrm{d}\Omega=\boldsymbol{D_y}\dot{\widetilde{\boldsymbol{T}}}, \tag{23}$$

where the jth-component of the row vector $\boldsymbol{D_y}$ is

$$\begin{aligned}D_{y,j}=&\sum_{i=1}^{N}\Psi_{ij}\int_{\Gamma}\frac{T^{(i)}(\boldsymbol{z},\boldsymbol{y})}{r(\boldsymbol{z},\boldsymbol{y})}\frac{\partial r}{\partial\boldsymbol{n}}\mathrm{d}\Gamma\\&+\Psi_{(N+1)j}\Big(\int_{\Gamma}\frac{r_{,1}T^{(A1)}(\boldsymbol{z},\boldsymbol{y})}{r(\boldsymbol{z},\boldsymbol{y})}\frac{\partial r}{\partial\boldsymbol{n}}\mathrm{d}\Gamma+y_1\int_{\Gamma}\frac{T^{(A2)}(\boldsymbol{z},\boldsymbol{y})}{r(\boldsymbol{z},\boldsymbol{y})}\frac{\partial r}{\partial\boldsymbol{n}}\mathrm{d}\Gamma\Big)\\&+\Psi_{(N+2)j}\Big(\int_{\Gamma}\frac{r_{,2}T^{(A1)}(\boldsymbol{z},\boldsymbol{y})}{r(\boldsymbol{z},\boldsymbol{y})}\frac{\partial r}{\partial\boldsymbol{n}}\mathrm{d}\Gamma+y_2\int_{\Gamma}\frac{T^{(A2)}(\boldsymbol{z},\boldsymbol{y})}{r(\boldsymbol{z},\boldsymbol{y})}\frac{\partial r}{\partial\boldsymbol{n}}\mathrm{d}\Gamma\Big)\\&+\Psi_{(N+3)j}\Big(\int_{\Gamma}\frac{T^{(A2)}(\boldsymbol{z},\boldsymbol{y})}{r(\boldsymbol{z},\boldsymbol{y})}\frac{\partial r}{\partial\boldsymbol{n}}\mathrm{d}\Gamma\Big),\end{aligned} \tag{24}$$

where the meaning of Ψ_{ij} can be found in Ref. [27], and

$$T^{(i)}(\boldsymbol{z},\boldsymbol{y})=\int_0^{r(\boldsymbol{z},\boldsymbol{y})}\frac{c(T)}{k(T)}G(\boldsymbol{x},\boldsymbol{y})\phi_i\xi\mathrm{d}\xi, \tag{25}$$

$$T^{(A1)}(\boldsymbol{z},\boldsymbol{y})=\int_0^{r(\boldsymbol{z},\boldsymbol{y})}\frac{c(T)}{k(T)}G(\boldsymbol{x},\boldsymbol{y})\xi^2\mathrm{d}\xi, \tag{26}$$

$$T^{(A2)}(\boldsymbol{z},\boldsymbol{y})=\int_0^{r(\boldsymbol{z},\boldsymbol{y})}\frac{c(T)}{k(T)}G(\boldsymbol{x},\boldsymbol{y})\xi\mathrm{d}\xi. \tag{27}$$

The same approximation procedure is done for the first domain integral in Eq. (18),

$$\widetilde{T}(\boldsymbol{x},t)=\sum_{i=1}^{N}\beta_i\phi_i(R)+\overline{\beta}_1x_1+\overline{\beta}_2x_2+\overline{\beta}_3. \tag{28}$$

The domain integral can be transformed as follows:

$$\int_{\Omega}\widetilde{T}(\boldsymbol{x},t)v(\boldsymbol{x},\boldsymbol{y},T)\mathrm{d}\Omega=\boldsymbol{V_y}\widetilde{\boldsymbol{T}}, \tag{29}$$

where the jth-component of the row vector $\boldsymbol{V_y}$ is

$$\begin{aligned}V_{y,j}=&\sum_{i=1}^{N}\Psi_{ij}\int_{\Gamma}\frac{V^{(i)}(\boldsymbol{z},\boldsymbol{y})}{r(\boldsymbol{z},\boldsymbol{y})}\frac{\partial r}{\partial\boldsymbol{n}}\mathrm{d}\Gamma\\&+\Psi_{(N+1)j}\Big(\int_{\Gamma}\frac{r_{,1}V^{(A1)}(\boldsymbol{z},\boldsymbol{y})}{r(\boldsymbol{z},\boldsymbol{y})}\frac{\partial r}{\partial\boldsymbol{n}}\mathrm{d}\Gamma+y_1\int_{\Gamma}\frac{V^{(A2)}(\boldsymbol{z},\boldsymbol{y})}{r(\boldsymbol{z},\boldsymbol{y})}\frac{\partial r}{\partial\boldsymbol{n}}\mathrm{d}\Gamma\Big)\\&+\Psi_{(N+2)j}\Big(\int_{\Gamma}\frac{r_{,2}V^{(A1)}(\boldsymbol{z},\boldsymbol{y})}{r(\boldsymbol{z},\boldsymbol{y})}\frac{\partial r}{\partial\boldsymbol{n}}\mathrm{d}\Gamma+y_2\int_{\Gamma}\frac{V^{(A2)}(\boldsymbol{z},\boldsymbol{y})}{r(\boldsymbol{z},\boldsymbol{y})}\frac{\partial r}{\partial\boldsymbol{n}}\mathrm{d}\Gamma\Big)\\&+\Psi_{(N+3)j}\Big(\int_{\Gamma}\frac{V^{(A2)}(\boldsymbol{z},\boldsymbol{y})}{r(\boldsymbol{z},\boldsymbol{y})}\frac{\partial r}{\partial\boldsymbol{n}}\mathrm{d}\Gamma\Big),\end{aligned} \tag{30}$$

where

$$V^{(i)}(\boldsymbol{z},\boldsymbol{y})=\int_0^{r(\boldsymbol{z},\boldsymbol{y})} v\phi_i\xi \mathrm{d}\xi, \tag{31}$$

$$V^{(A1)}(\boldsymbol{z},\boldsymbol{y})=\int_0^{r(\boldsymbol{z},\boldsymbol{y})} v\xi^2 \mathrm{d}\xi, \tag{32}$$

$$V^{(A2)}(\boldsymbol{z},\boldsymbol{y})=\int_0^{r(\boldsymbol{z},\boldsymbol{y})} v\xi \mathrm{d}\xi. \tag{33}$$

Substituting Eqs. (23) and (29) into Eq. (18), one can get the integral equation with only boundary integrals as follows:

$$\begin{aligned} c(\boldsymbol{y})\widetilde{T}(\boldsymbol{y})=&\int_\Gamma G(\boldsymbol{x},\boldsymbol{y})\frac{\partial \widetilde{T}(\boldsymbol{x},t)}{\partial x_i}n_i \mathrm{d}\Gamma-\int_\Gamma \widetilde{T}(\boldsymbol{x},t)\frac{\partial G(\boldsymbol{x},\boldsymbol{y})}{\partial x_i}n_i \mathrm{d}\Gamma\\ &+\rho \boldsymbol{V}_{\boldsymbol{y}}(T)\dot{\widetilde{\boldsymbol{T}}}-\int_\Gamma \frac{F(\boldsymbol{z},\boldsymbol{y})}{r(\boldsymbol{z},\boldsymbol{y})}\frac{\partial r}{\partial \boldsymbol{n}}\mathrm{d}\Gamma-\rho \boldsymbol{D}_{\boldsymbol{y}}(T)\dot{\widetilde{\boldsymbol{T}}}. \end{aligned} \tag{34}$$

The boundary Γ is discretized into N_e boundary elements with $N_{\mathrm{b}1}$ boundary nodes on Γ_1 and $N_{\mathrm{b}2}$ boundary nodes on Γ_2, which ensures that the total number of boundary nodes is $N_\mathrm{b}=N_{\mathrm{b}1}+N_{\mathrm{b}2}$, and N_i internal nodes are distributed into the domain Ω. The total number of nodes is $N=N_\mathrm{b}+N_\mathrm{i}$. Then, the temperature vector can be written as

$$\widetilde{\boldsymbol{T}}=\begin{pmatrix}\widetilde{\boldsymbol{T}}_\mathrm{b}\\ \widetilde{\boldsymbol{T}}_\mathrm{i}\end{pmatrix}=\begin{pmatrix}\widetilde{\boldsymbol{T}}_{\mathrm{b}1}\\ \widetilde{\boldsymbol{T}}_{\mathrm{b}2}\\ \widetilde{\boldsymbol{T}}_\mathrm{i}\end{pmatrix}=\begin{pmatrix}\widetilde{\boldsymbol{T}}_{\mathrm{b}1}\\ \boldsymbol{X}\end{pmatrix}. \tag{35}$$

After applying Eq. (34) on both boundary and internal nodes, the following differential equations are obtained:

$$\boldsymbol{C}_{\boldsymbol{y}}\widetilde{\boldsymbol{T}}_\mathrm{b}=\boldsymbol{G}_\mathrm{b}\boldsymbol{q}_\mathrm{b}-\widehat{\boldsymbol{H}}_\mathrm{b}\widetilde{\boldsymbol{T}}_\mathrm{b}+\boldsymbol{V}_\mathrm{b}\dot{\widetilde{\boldsymbol{T}}}_\mathrm{b}-\boldsymbol{f}_\mathrm{b}-\boldsymbol{C}_\mathrm{b}\dot{\widetilde{\boldsymbol{T}}}, \tag{36}$$

$$\widetilde{\boldsymbol{T}}_\mathrm{i}=\boldsymbol{G}_\mathrm{i}\boldsymbol{q}_\mathrm{b}-\widehat{\boldsymbol{H}}_\mathrm{i}\widetilde{\boldsymbol{T}}_\mathrm{b}+\boldsymbol{V}_\mathrm{i}\dot{\widetilde{\boldsymbol{T}}}_\mathrm{b}-\boldsymbol{f}_\mathrm{i}-\boldsymbol{C}_\mathrm{i}\dot{\widetilde{\boldsymbol{T}}}, \tag{37}$$

where $\boldsymbol{C}_{\boldsymbol{y}}=\mathrm{diag}(c(\boldsymbol{y}_1),c(\boldsymbol{y}_2),\cdots,c(\boldsymbol{y}_{N_\mathrm{b}}))$, $\boldsymbol{G},\widehat{\boldsymbol{H}},\boldsymbol{V},\boldsymbol{f}$, and $\boldsymbol{C}$ are respectively generated by discretization of the five boundary integrals on the right-hand side of Eq. (34), and the subscripts 'b' and 'i' denote boundary nodes and internal nodes, respectively.

According to the boundary conditions, for $N_{\mathrm{b}1}$ boundary nodes whose $\widetilde{\boldsymbol{T}}_{\mathrm{b}1}$ and $\dot{\widetilde{\boldsymbol{T}}}_{\mathrm{b}1}$ are known, $\boldsymbol{q}_{\mathrm{b}1}$ is to be solved, and for $N_{\mathrm{b}2}$ boundary nodes whose $\boldsymbol{q}_{\mathrm{b}2}$ is known, $\widetilde{\boldsymbol{T}}_{\mathrm{b}2}$ and $\dot{\widetilde{\boldsymbol{T}}}_{\mathrm{b}2}$ are to be solved. According to the $N_{\mathrm{b}1}$ equations of Eq. (36), $\boldsymbol{q}_{\mathrm{b}1}$ can be eliminated[27]. Then, the differential equations, where the unknown vector $\boldsymbol{X}$ is involved, can be obtained,

$$\boldsymbol{A}(T)\dot{\boldsymbol{X}}=\boldsymbol{K}(T)\boldsymbol{X}+\boldsymbol{y}_\mathrm{b}(T). \tag{38}$$

4 Procedures of predictor-corrector PIM

In order to use the PIM to solve Eq. (38), in the time interval $[t_k,t_{k+1}]$, Eq. (38) can be rewritten as

$$\boldsymbol{A}_0\dot{\boldsymbol{X}}=\boldsymbol{K}_0\boldsymbol{X}+(\boldsymbol{K}(T)-\boldsymbol{K}_0)\boldsymbol{X}-(\boldsymbol{A}(T)-\boldsymbol{A}_0)\dot{\boldsymbol{X}}+\boldsymbol{y}_\mathrm{b}(T), \tag{39}$$

where $\boldsymbol{A}_0=\boldsymbol{A}(T(t_k))$, and $\boldsymbol{K}_0=\boldsymbol{K}(T(t_k))$.

Then, one can obtain

$$\dot{\boldsymbol{X}}=\boldsymbol{B}\boldsymbol{X}+\boldsymbol{r}_\mathrm{i}, \tag{40}$$

where $\boldsymbol{B}=\boldsymbol{A}_0^{-1}\boldsymbol{K}_0$, and $\boldsymbol{r}_{\mathrm{i}}=\boldsymbol{A}_0^{-1}(\boldsymbol{K}-\boldsymbol{K}_0)\boldsymbol{X}-\boldsymbol{A}_0^{-1}\boldsymbol{A}\dot{\boldsymbol{X}}+\dot{\boldsymbol{X}}+\boldsymbol{A}_0^{-1}\boldsymbol{y}_{\mathrm{b}}$.

The general solution to Eq. (40) is

$$\boldsymbol{X}(t_{k+1})=\exp(\boldsymbol{B}\Delta t)\boldsymbol{X}(t_k)+\int_0^{\Delta t}\exp(\boldsymbol{B}(\Delta t-\tau))\boldsymbol{r}_{\mathrm{i}}(t_k+\tau,\boldsymbol{T})\mathrm{d}\tau, \tag{41}$$

where $\Delta t=t_{k+1}-t_k$.

The calculation of Eq. (41) is carried out by the predictor-corrector iteration technique[28] as follows.

Step 1 Let $n_{\mathrm{iter}}=0$, and do the following calculation:

$$\boldsymbol{X}_{k+1,0}=\boldsymbol{X}_{\mathrm{e}}+\boldsymbol{E}\boldsymbol{K}^{-1}\boldsymbol{r}_{\mathrm{i}0}-\boldsymbol{K}^{-1}\boldsymbol{r}_{\mathrm{i}0}, \tag{42}$$

where $\boldsymbol{X}_{\mathrm{e}}=\boldsymbol{E}\boldsymbol{X}(t_k)$, $\boldsymbol{E}=\exp(\boldsymbol{B}\Delta t)$, $\boldsymbol{K}=\boldsymbol{K}(\boldsymbol{T}(\boldsymbol{X}_{\mathrm{e}}))$, and $\boldsymbol{r}_{\mathrm{i}0}=\boldsymbol{r}_{\mathrm{i}}(t_k,\boldsymbol{T}_k)$.

Step 2 Let $n_{\mathrm{iter}}:=n_{\mathrm{iter}}+1$, and assume that $\boldsymbol{r}_{\mathrm{i}}$ is linear with respect to t, which is expressed as

$$\boldsymbol{r}_{\mathrm{i}}=\boldsymbol{r}_{\mathrm{i}}(t_k,T_k)+\theta(\tau/\Delta t)(\boldsymbol{r}_{\mathrm{i}}(t_{k+1},T_{k+1,n_{\mathrm{iter}}-1})-\boldsymbol{r}_{\mathrm{i}}(t_k,T_k)), \tag{43}$$

where $0<\tau\leqslant\Delta t$, θ is the relaxing factor, and $0<\theta\leqslant 1$, which is taken as 0.5 in the calculation processes of the numerical examples of this paper.

Do the following calculation:

$$\boldsymbol{X}_{k+1,n_{\mathrm{iter}}}=\boldsymbol{E}\boldsymbol{X}(t_k)+\boldsymbol{E}\boldsymbol{K}^{-1}(\boldsymbol{r}_{\mathrm{i}0}+\boldsymbol{K}^{-1}\boldsymbol{r}_{\mathrm{i}1})-\boldsymbol{K}^{-1}(\boldsymbol{r}_{\mathrm{i}0}+\boldsymbol{K}^{-1}\boldsymbol{r}_{\mathrm{i}1}+\Delta t\boldsymbol{r}_{\mathrm{i}1}), \tag{44}$$

where $\boldsymbol{r}_{\mathrm{i}0}=\boldsymbol{r}_{\mathrm{i}}(t_k,T_k)$, and $\boldsymbol{r}_{\mathrm{i}1}=\theta(\boldsymbol{r}_{\mathrm{i}}(t_{k+1},T_{k+1,n_{\mathrm{iter}}-1})-\boldsymbol{r}_{\mathrm{i}0})/\Delta t$.

Step 3 Check the convergence. If $\|\boldsymbol{X}_{k+1,n_{\mathrm{iter}}}-\boldsymbol{X}_{k+1,n_{\mathrm{iter}}-1}\|_2<\varepsilon$ (where $\|\cdot\|_2$ denotes a vector's 2-norm, and ε is a prespecified acceptable error), the convergence is achieved, $\boldsymbol{X}_{k+1,n_{\mathrm{iter}}}$ is the solution at t_{k+1}, and then go to the next time step. Otherwise, go to Step 2.

After $\boldsymbol{X}(t_{k+1})$ is obtained, the temperature field and temperature gradient at t_{k+1} are all known. Then, the moving interface needs to be tracked.

5 Numerical steps of front-tracking method

To determine the position of the interface, the moving velocity and the direction are needed. The moving velocity can be calculated by Eq. (8) once the heat flux on the solid-mushy interface is obtained. The moving direction can be determined by a length weighted unite normal vector as the following equation[6,29]:

$$\overline{\boldsymbol{n}}_j=(l_{i-1}\boldsymbol{n}_{i-1}+l_i\boldsymbol{n}_i)/(l_{i-1}+l_i),\quad \boldsymbol{n}_j=\overline{\boldsymbol{n}}_j/\left\|\overline{\boldsymbol{n}}_j\right\|_2, \tag{45}$$

where the subscript j indicates the jth-node on the moving interface, the subscripts $i-1$ and i indicate the two adjacent boundary elements of the jth-node on the moving interface, l_{i-1} and l_i denote the lengths of these adjacent boundary elements, and $\|\cdot\|_2$ denotes a vector's 2-norm.

The position of the moving interface can be obtained by an iterative algorithm. The front-tracking procedures in one time step $[t_k,t_{k+1}]$ are described in detail by the following steps.

Step 1 Specify a tiny distance Δs beforehand for the purpose of controlling the maximum moving distance of Γ_{ms}.

Step 2 At the initial time t_k, the heat flux $\boldsymbol{q}(t_k)$ at all the boundaries is obtained from the results of the last time step, boundary conditions, or initial conditions. Then, the normal velocity $V_j(t_k)$ of the jth-node on the moving interface Γ_{ms} at t_k can be calculated by Eq. (8), and $\boldsymbol{V}(t_k)=\{V_j(t_k)\}$.

Step 3 The time step Δt_{k+1} is determined by the following equation:

$$\Delta t_{k+1} = \Delta s \rho L / \|\boldsymbol{V}(t_k)\|_\infty, \tag{46}$$

where $\|\cdot\|_\infty$ denotes a vector's infinity norm, and $t_{k+1} = t_k + \Delta t_{k+1}$.

Step 4 Estimate $\boldsymbol{V}^{\mathrm{p}}(t_{k+1}) = 0.7\boldsymbol{V}(t_k)$, where $\boldsymbol{V}^{\mathrm{p}}(t_{k+1})$ denotes the predicted velocity of the moving interface Γ_{ms} at t_{k+1}.

Step 5 Calculate the predicted position of the jth-node on Γ_{ms} at t_{k+1} by

$$\boldsymbol{x}_j(t_{k+1}) = \boldsymbol{x}_j(t_k) + \Delta t_{k+1}(V_j(t_k) + V_j^{\mathrm{p}}(t_{k+1}))\boldsymbol{n}_j/2, \tag{47}$$

and update the geometry at t_{k+1}.

Step 6 Apply the radial integration BEM in the solid domain and non-solid domain, and then use the procedures described in the last section to calculate the temperature at t_{k+1} by the PIM.

Step 7 Calculate the unknown heat flux at t_{k+1} in the solid domain and the non-solid domain, respectively, and then calculate the normal velocity $V_j(t_{k+1})$ of the jth-node on the moving interface Γ_{ms} at t_{k+1} by Eq. (10), and $\boldsymbol{V}(t_{k+1}) = \{V_j(t_{k+1})\}$.

Step 8 Check the convergence. If $\|\boldsymbol{V}(t_{k+1}) - \boldsymbol{V}^{\mathrm{p}}(t_{k+1})\|_2 / \|\boldsymbol{V}(t_{k+1}) + \boldsymbol{V}(t_k)\|_2 \leqslant \varepsilon$, where ε is a prespecified acceptable error, the convergence is achieved. Otherwise, let $\boldsymbol{V}^{\mathrm{p}}(t_{k+1}) = \boldsymbol{V}(t_{k+1})$, and then go to Step 5.

Step 9 The position of Γ_{ms} obtained in Step 5 and the temperatures calculated in Step 6 are assumed to be the results at t_{k+1}. Obtain the mushy-liquid interface by interpolation of temperature field. Do the re-meshing. Add or delete the boundary elements, boundary nodes, and internal nodes in both solid and non-solid domains if needed. Let $t_k := t_{k+1}$, and go to Step 1. Execute the iterative algorithm for the next time step until the ending time is reached.

6 Numerical examples

In the numerical processes, the heat capacities and thermal conductivities are assumed to be constant in the solid domain and the liquid domain, but linear with respect to temperature in the mushy zone[30], which are given by

$$k_{\mathrm{m}} = fk_{\mathrm{s}} + (1-f)k_{\mathrm{l}}, \quad c_{\mathrm{m}} = fc_{\mathrm{s}} + (1-f)c_{\mathrm{l}}, \tag{48}$$

where f is assumed to be linear with respect to temperature as follows:

$$f = f_{\mathrm{su}}\Big(1 - \frac{T(\boldsymbol{x},t) - T_{\mathrm{ms}}}{T_{\mathrm{ml}} - T_{\mathrm{ms}}}\Big). \tag{49}$$

Four numerical examples for the phase change problems with the mushy zone are presented to assess the performance of the proposed numerical algorithm. Analytical solutions are used as reference for Example 1, while the solutions by a combination of fixed-domain method and FEM are used as reference for Example 2, Example 3, and Example 4.

Example 1 The freezing problem in a cylindrical symmetry region with an extended freezing temperature range is studied. The considered region is liquid initially with the constant temperature T_0 ($T_0 > T_{\mathrm{ml}}$). When $t > 0$ s, a heat sink of strength Q is located at $r = 0$. According to Ref. [25], the analytical solutions of the solid-mushy interface and liquid-mushy interface are given by

$$s_{\mathrm{ms}}(t) = 2\lambda\sqrt{\alpha_{\mathrm{s}} t}, \quad s_{\mathrm{ml}}(t) = 2\eta\sqrt{\alpha_{\mathrm{s}}^* t}. \tag{50}$$

The analytical solutions of the temperature field are given by

$$T_{\mathrm{s}}(r,t) = T_{\mathrm{ms}} + \frac{Q}{4\pi k_{\mathrm{s}}}(E_{\mathrm{i}}(-r^2/(4\alpha_{\mathrm{s}} t)) - E_{\mathrm{i}}(-\lambda^2)), \tag{51}$$

$$T_{\mathrm{m}}(r,t)=\frac{(T_{\mathrm{ms}}-T_{\mathrm{ml}})E_{\mathrm{i}}(-r^2/(4\alpha_{\mathrm{s}}t))+T_{\mathrm{ms}}E_{\mathrm{i}}(-\eta^2)-T_{\mathrm{ml}}E_{\mathrm{i}}(-\lambda^2\alpha_{\mathrm{s}}/\alpha^*_{\mathrm{ms}})}{E_{\mathrm{i}}(-\eta^2)-E_{\mathrm{i}}(-\lambda^2\alpha_{\mathrm{s}}/\alpha^*_{\mathrm{ms}})}, \tag{52}$$

$$T_{\mathrm{l}}(r,t)=T_0-(T_0-T_{\mathrm{ml}})E_{\mathrm{i}}(-r^2/(4\alpha_{\mathrm{s}}t))/E_{\mathrm{i}}(-\eta^2\alpha_{\mathrm{s}}/\alpha^*_{\mathrm{ms}}), \tag{53}$$

where $E_{\mathrm{i}}(x)$ is the first-order exponential integral function, $\alpha_{\mathrm{s}}=k_{\mathrm{s}}/(\rho c_{\mathrm{s}})$, $\alpha_{\mathrm{m}}=k_{\mathrm{m}}/(\rho c_{\mathrm{m}})$, and $\alpha^*_{\mathrm{ms}}=(\alpha_{\mathrm{m}}k_{\mathrm{m}}(T_{\mathrm{ml}}-T_{\mathrm{ms}}))/(\rho L f_{\mathrm{su}}\alpha_{\mathrm{m}}+k_{\mathrm{m}}(T_{\mathrm{ml}}-T_{\mathrm{ms}}))$.

This problem can be approximated by an annulus region $0.1<r<1$ as shown in Fig. 2. Consider the phase change material-1 (PCM-1) as shown in Table 1. The initial condition is specified by

$$T(r,0)=T_0=10. \tag{54}$$

The boundary conditions are specified by

$$T(0.1,t)=T_{\mathrm{s}}(0.1,t),\quad T(1,t)=T_{\mathrm{s}}(1,t). \tag{55}$$

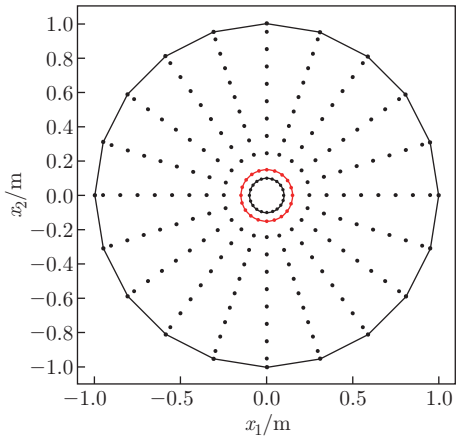

Fig. 2 Element and node schematic diagram of Example 1 (color online)

Table 1 Thermo-physical properties of the phase change materials

Property	PCM-1	PCM-2	PCM-3	PCM-4
$T_{\mathrm{ms}}/^\circ\mathrm{C}$	−1	1	1	20
$T_{\mathrm{ml}}/^\circ\mathrm{C}$	1	2	2	24
$\rho/(\mathrm{kg}\cdot\mathrm{m}^{-3})$	1	1	1	880
f_{su}	0.5	0.5	0.5	0.5
$L/(\mathrm{J}\cdot\mathrm{kg}^{-1})$	10	1	1	200 000
$c_{\mathrm{s}}/(\mathrm{J}\cdot\mathrm{kg}^{-1}\cdot\mathrm{K}^{-1})$	1	1	1	2 000
$c_{\mathrm{m}}/(\mathrm{J}\cdot\mathrm{kg}^{-1}\cdot\mathrm{K}^{-1})$	1	1	1	2 000
$c_{\mathrm{l}}/(\mathrm{J}\cdot\mathrm{kg}^{-1}\cdot\mathrm{K}^{-1})$	1	1	1	2 000
$k_{\mathrm{s}}/(\mathrm{W}\cdot\mathrm{m}^{-1}\cdot\mathrm{K}^{-1})$	1	1	1	0.2
$k_{\mathrm{m}}/(\mathrm{W}\cdot\mathrm{m}^{-1}\cdot\mathrm{K}^{-1})$	1	1	1	0.2
$k_{\mathrm{l}}/(\mathrm{W}\cdot\mathrm{m}^{-1}\cdot\mathrm{K}^{-1})$	1	1	1	0.2

The thermal-physical properties, the initial condition, and the boundary conditions determine $\lambda=0.343\,331$, and $\eta=0.758\,593$.

The relative errors of the interface positions of the present method and the analytical solutions are shown in Figs. 3 and 4 when Δs is different, and the total number of nodes is 320. The maximum relative error of the solid-mushy interface position is 4.29%, while the maximum relative error of the liquid-mushy interface position is 2.79%. The relative errors

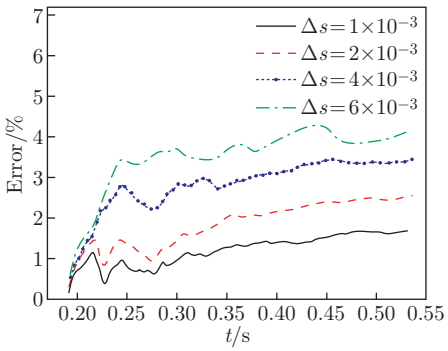

Fig. 3 Relative errors of solid-mushy interface position of Example 1 (color online)

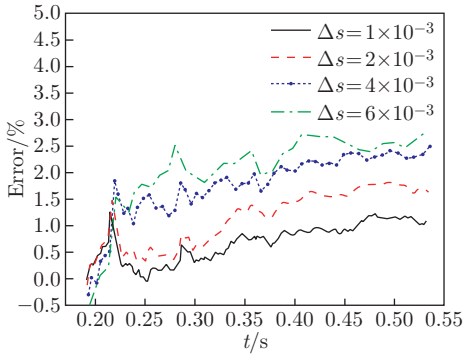

Fig. 4 Relative errors of liquid-mushy interface position of Example 1 (color online)

of the solid-mushy interface positions of the present method and the analytical solutions are shown in Fig. 5, when the total number of nodes is different, and $\Delta s = 4 \times 10^{-3}$. The maximum relative error of the solid-mushy interface position is 3.45%. If the total number of nodes is 320, the maximum relative error of the solid-mushy interface position is 0.99%. It can be found that the results of the present method agree well with the analytical solutions, and both the decrease in the step Δs and the increase in the total number of BEM nodes would increase the accuracy. The present method is coded by MATLAB and computed by Intel Core i5-4460 CPU, and the CPU time is listed in Table 2.

Table 2 CPU time of Example 1

Total number of nodes	96	176	320
CPU time/s	155.0	462.9	1 280.7

Example 2 A solidification problem of a 1×1 domain is studied as shown in Fig. 6. The considered domain is full of PCM with the constant initial temperature $T_0 = 3\,^{\circ}\mathrm{C}$. When $t > 0$ s, a temperature boundary condition $T_{\mathrm{w}} = 0\,^{\circ}\mathrm{C}$ is applied at $x_1 = 0$ m and $x_2 = 0$ m. Consider the properties of the PCM-2 in Table 1.

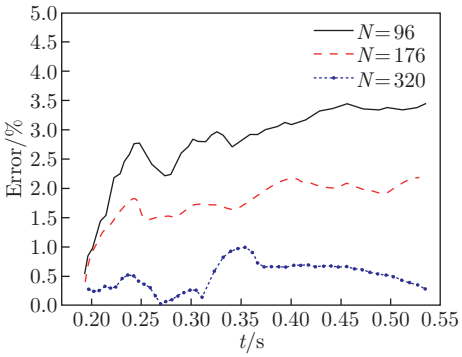

Fig. 5 Relative errors of Example 1 with different numbers of nodes (color online)

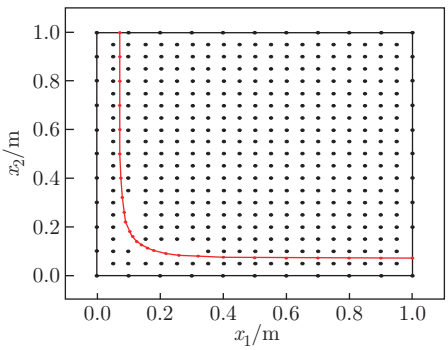

Fig. 6 Element and node schematic diagram of Example 2 (color online)

The locations of the interface at various time are shown in Fig. 7, where 'S-BEM' and 'L-BEM' represent the BEM for solid-mushy interfaces and liquid-mushy interfaces, respectively.

It can be found that there is good agreement between the interface position results of the present method and the FEM solutions.

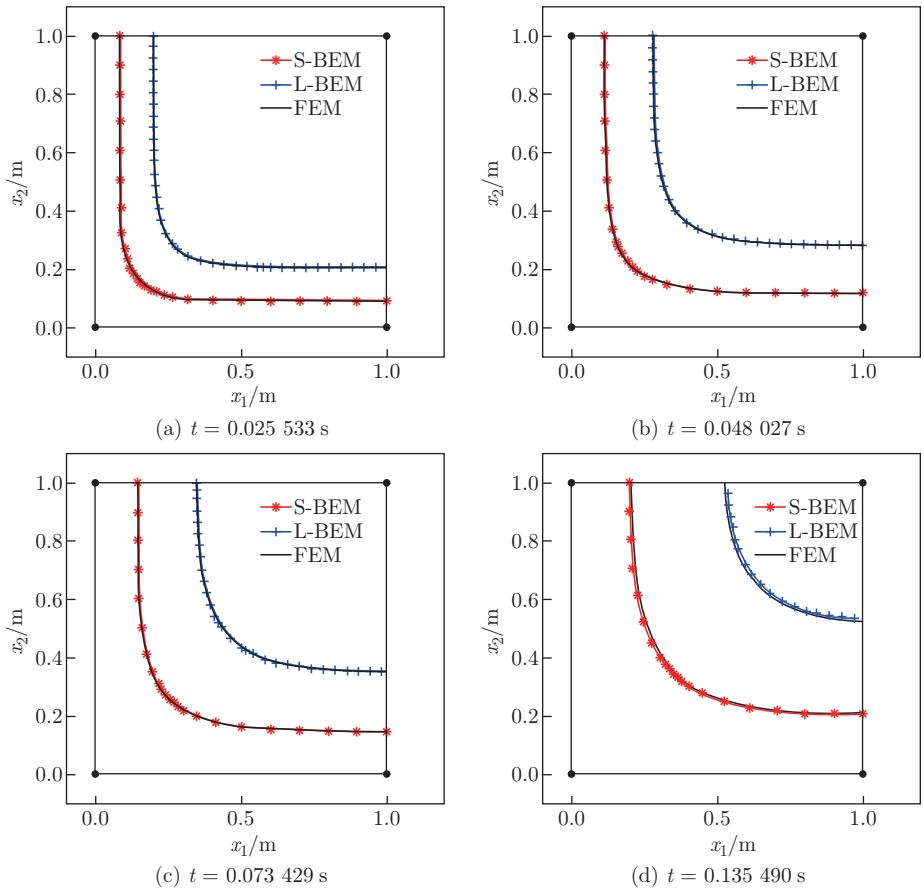

(a) $t = 0.025\ 533$ s (b) $t = 0.048\ 027$ s

(c) $t = 0.073\ 429$ s (d) $t = 0.135\ 490$ s

Fig. 7 Interface positions of Example 2 (color online)

Example 3 The solidification problem of a phase change heat storage system as shown in Fig. 8 is studied. The considered region is full of PCM with the constant initial temperature $T_0 = 3$ °C. When $t > 0$ s, a temperature boundary condition $T_w = 0$ °C is applied at both the interior and exterior walls. Consider the properties of the PCM-3 in Table 1.

The locations of the interface at various time are shown in Figs. 9–12. It can be found that there is good agreement between the interface position results of the present method and the FEM solutions. The topology change of the solid domain can be seen from Fig. 10. From Figs. 11 and 12, the topology changes of the liquid domain can also be found. The proposed method can solve phase change problems with topology changes for both the solid domain and the liquid domain accurately.

Example 4 The solidification problem of a phase change heat storage system as shown in Fig. 13 is studied. The area between the interior and exterior copper walls with fins is occupied by the PCM, where the phase change takes place. The initial temperature of the considered domain is $T_0 = 40$ °C. When $t > 0$ s, a temperature boundary condition $T_w = 15$ °C is applied at both the interior and exterior walls. Consider the properties of the PCM-4 in Table 1. In the copper domain, the thermal conductivity is 400 W/(m · K), the specific heat is 380 J/(kg · K), and the density is 8 920 kg/m^3.

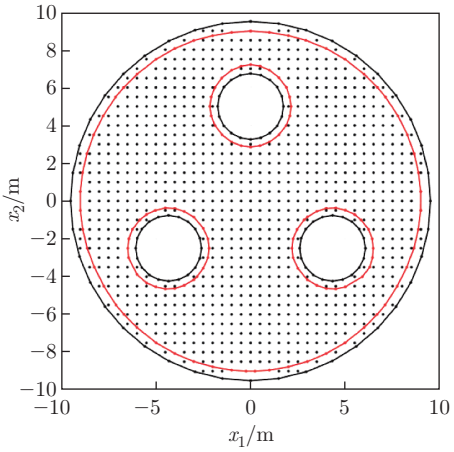

Fig. 8 Element and node schematic diagram of Example 3 (color online)

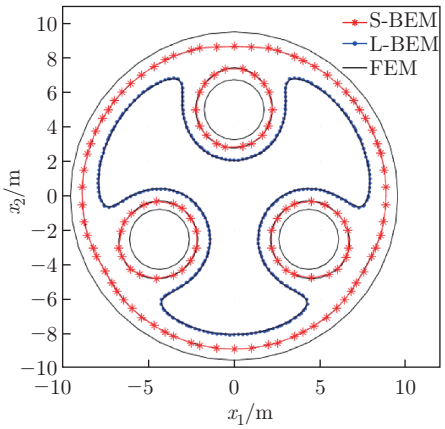

Fig. 9 Interface positions of Example 3 when $t = 1.298\,6$ s (color online)

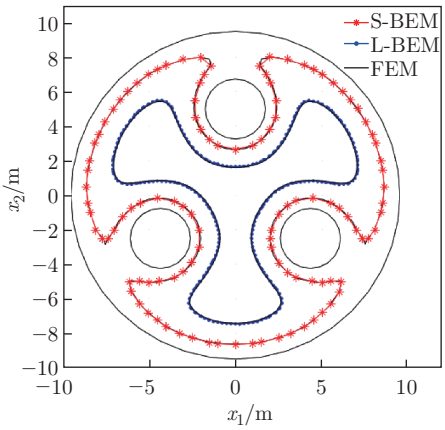

Fig. 10 Interface positions of Example 3 when $t = 2.174\,9$ s (color online)

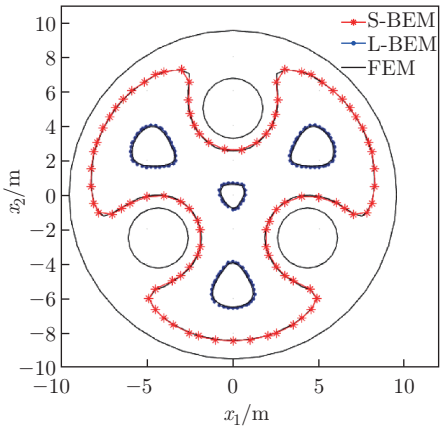

Fig. 11 Interface positions of Example 3 when $t = 3.175\,2$ s (color online)

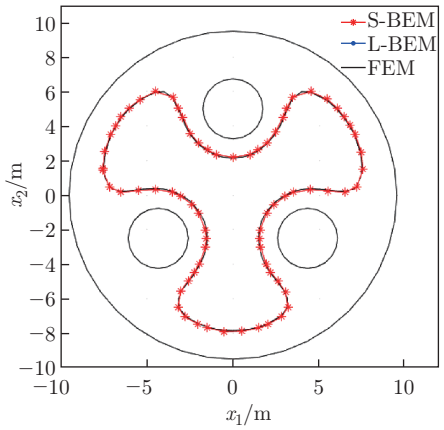

Fig. 12 Interface positions of Example 3 when $t = 5.302\,2$ s (color online)

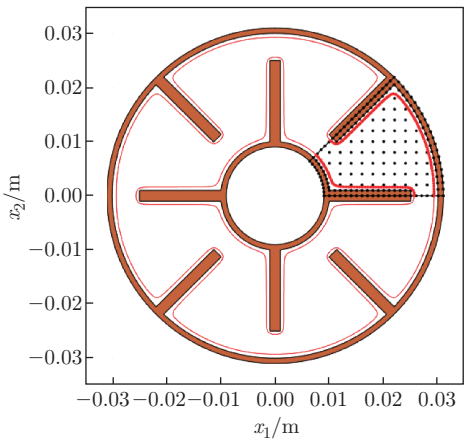

Fig. 13 Element and node schematic diagram of Example 4 (color online)

There is not any phase change in the copper domain, but the heat conduction in this domain needs to be considered and numerically analyzed. The BEM is applied in the copper domain and the adjoining PCM domain, respectively, to get two sets of differential equations. At the interface between the copper domain and the PCM domain, the temperature is continuous, and the heat flux is equilibrated. Therefore, according to this interface condition, these two sets of equations can be assembled into one. Then, the PIM results of temperature and heat flux can be obtained for both the copper domain and PCM domain.

Because of the symmetry, only 1/8 part of the storage device is considered in the numerical calculation. The locations of the interface at various time are shown in Fig. 14. It can be found that there is good agreement between the interface position results of the present method and the FEM solutions. The topology change of the solid domain can be seen from Figs. 14(b) and 14(c). The topology change of the liquid domain can be seen from Fig. 14(b). The proposed method can solve phase change problems with topology changes and multi-medium heat conduction accurately.

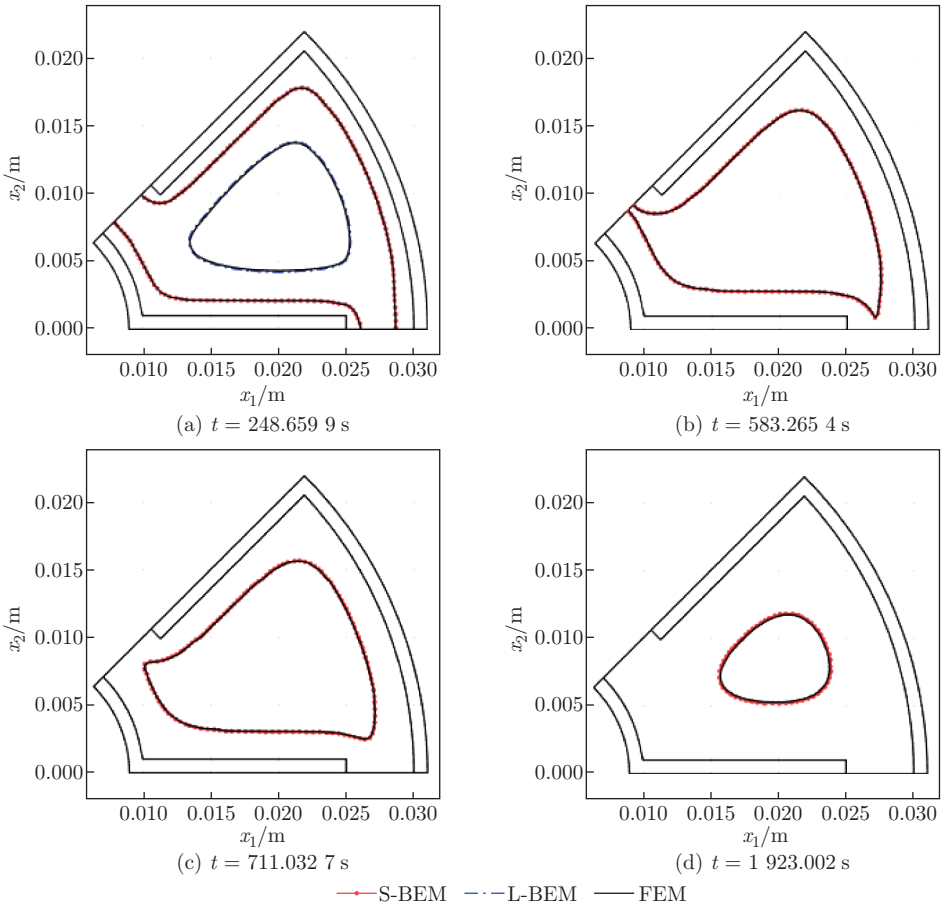

Fig. 14 Interface positions of Example 4 (color online)

7 Conclusions

This article proposes a precise integration BEM to solve the phase change problem with the mushy zone. The changes of latent heat are approximated by heat source, and the liquid

phase and the mushy zone are considered as a whole part. The front-tracking method is used to track the move of the interface between the solid phase and the mushy zone, and the interface between the liquid phase and the mushy zone is obtained by interpolation of the temperature field.

Compared with the reference solutions, the results of the numerical examples show that the proposed method can determine the phase change interface positions correctly. It can be found that both the step Δs and the number of BEM nodes would influence the computing accuracy dramatically. The proposed scheme is very convenient to be applied in the moving-mesh of the grid, and can properly deal with topology changes including separation merging and vanishment. It can also deal with multi-medium problems by carrying out the BEM in different domains. It is reliable and accurate to apply the proposed numerical method for solving phase change problems with mushy zones.

References

[1] HONG, Y., YE, W., DU, J., and HUANG, S. Solid-liquid phase-change thermal storage and release behaviors in a rectangular cavity under the impacts of mushy region and low gravity. *International Journal of Heat and Mass Transfer*, **130**, 1120–1132 (2019)

[2] CRANK, J. *Free and Moving Boundary Problems*, Clarendon Press, Oxford (1984)

[3] HE, Y., DONG, X., and YANG, H. A new adaptive algorithm for phase change heat transfer problems based on quadtree SBFEM and smoothed effective heat capacity method. *Numerical Heat Transfer*, *Part B*: *Fundamentals*, **75**(2), 111–126 (2019)

[4] ZHAO, X. and CHEN, X. The temperature analysis of the billet with phase change during continuous casting. *Applied Mathematics and Mechanics* (*English Edition*), **15**(2), 109–118 (1994) https://doi.org/10.1007/BF02451045

[5] LI, F., LIU, J., and YUE, K. Exact analytical solution to three-dimensional phase change heat transfer problems in biological tissues subject to freezing. *Applied Mathematics and Mechanics* (*English Edition*), **30**(1), 63–72 (2009) https://doi.org/10.1007/s10483-009-0107-x

[6] YAO, W., WANG, Z., ZUO, C., and HU, X. Precise time-domain expanding boundary element method for solving phase change problems. *Numerical Heat Transfer*, *Part B*: *Fundamentals*, **76**(4), 203–223 (2019)

[7] YU, B., YAO, W. A., GAO, X. W., and ZHANG, S. Radial integration BEM for one-phase solidification problems. *Engineering Analysis with Boundary Elements*, **39**, 36–43 (2014)

[8] LI, Y. and ZHANG, Z. Solving the free boundary problem in continuous casting by using boundary element method. *Applied Mathematics and Mechanics* (*English Edition*), **16**(12), 1201–1208 (1995) https://doi.org/10.1007/BF02466990

[9] CHESSA, J., SMOLINSKI, P., and BELYTSCHKO, T. The extended finite element method (XFEM) for solidification problems. *International Journal for Numerical Methods in Engineering*, **53**(8), 1959–1977 (2002)

[10] ZHOU, J. and QI, L. Treatment of discontinuous interface in liquid-solid forming with extended finite element method. *Transactions of Nonferrous Metals Society of China*, **20**, s911–s915 (2010)

[11] HE, M., YANG, Q., LI, N., FENG, X., and LIU, N. An extended finite element method for heat transfer with phase change in frozen soil. *Soil Mechanics and Foundation Engineering*, **57**(6), 497–505 (2021)

[12] LIAO, J. and ZHUANG, Z. A consistent projection-based SUPG/PSPG XFEM for incompressible two-phase flows. *Acta Mechanica Sinica*, **28**(5), 1309–1322 (2012)

[13] YU, B., XU, C., YAO, W., and MENG, Z. Estimation of boundary condition on the furnace inner wall based on precise integration BEM without iteration. *International Journal of Heat and Mass Transfer*, **122**, 823–845 (2018)

[14] YANG, K., LI, H., PENG, H., and GAO, X. New interface integration BEM for solving multi-medium nonlinear heat transfer problems. *Engineering Analysis with Boundary Elements*, **117**, 66–75 (2020)

[15] ANG, W. T. and WANG, X. A numerical method based on boundary integral equations and radial basis functions for plane anisotropic thermoelastostatic equations with general variable coefficients. *Applied Mathematics and Mechanics* (*English Edition*), **41**(4), 551–566 (2020) https://doi.org/10.1007/s10483-020-2592-8

[16] YU, B., ZHOU, H. L., GAO, Q., and YAN, J. Geometry boundary identification of the furnace inner wall by BEM without iteration. *Numerical Heat Transfer*, *Part A*: *Applications*, **69**(11), 1253–1262 (2016)

[17] CHOLEWA, R., NOWAK, A. J., and WROBEL, L. C. Application of BEM and sensitivity analysis to the solution of the governing diffusion-convection equation for a continuous casting process. *Engineering Analysis with Boundary Elements*, **28**(4), 389–403 (2004)

[18] WANG, Z., YAO, W., ZUO, C., and HU, X. Solving phase change problems via a precise time-domain expanding boundary element method combined with the level set method. *Engineering Analysis with Boundary Elements*, **126**, 1–12 (2021)

[19] YU, B., TONG, Y., HU, P., and GAO, Q. A novel inversion approach for identifying the shape of cavity by combining Gappy POD with direct inversion scheme. *International Journal of Heat and Mass Transfer*, **150**, 119365 (2020)

[20] GAO, X. The radial integration method for evaluation of domain integrals with boundary-only discretization. *Engineering Analysis with Boundary Elements*, **26**(10), 905–916 (2002)

[21] YANG, K., LIU, Y., and GAO, X. Analytical expressions for evaluation of radial integrals in stress computation of functionally graded material problems using RIBEM. *Engineering Analysis with Boundary Elements*, **44**, 98–103 (2014)

[22] AL-BAYATI, S. A. and WROBEL, L. C. Radial integration boundary element method for two-dimensional non-homogeneous convection-diffusion-reaction problems with variable source term. *Engineering Analysis with Boundary Elements*, **101**, 89–101 (2019)

[23] ZHONG, W. X. On precise time-integration method for structural dynamics (in Chinese). *Journal of Dalian University of Technology*, **34**(02), 131–136 (1994)

[24] ZHANG, H., CHEN, B., and GU, Y. An adaptive algorithm of precise integration for transient analysis. *Acta Mechanica Solida Sinica*, **14**(3), 215–224 (2001)

[25] OZISIK, M. N. and UZZELL, J. C. Exact solution for freezing in cylindrical symmetry with extended freezing temperature range. *Journal of Heat Transfer*, **101**(2), 331–334 (1979)

[26] YU, B., YAO, W. A., and GAO, Q. A precise integration boundary-element method for solving transient heat conduction problems with variable thermal conductivity. *Numerical Heat Transfer*, *Part B*: *Fundamentals*, **65**(5), 472–493 (2014)

[27] YAO, W., YAO, H., ZUO, C., and HU, X. Precise integration boundary element method for solving dual phase change problems based on the effective heat capacity model. *Engineering Analysis with Boundary Elements*, **108**, 411–421 (2019)

[28] GU, Y. X., CHEN, B. S., ZHANG, H. W., and GUAN, Z. Q. Precise time integration method for solution of nonlinear transient heat conduction (in Chinese). *Journal of Dalian University of Technology*, **40**(1), 24–28 (2000)

[29] O'NEILL, K. Boundary integral equation solution of moving boundary phase change problems. *International Journal for Numerical Methods in Engineering*, **19**(12), 1825–1850 (1983)

[30] LIN, J. Y. and CHEN, H. T. Numerical analysis for phase change problems with the mushy zone. *Numerical Heat Transfer*, *Part A*: *Applications*, **27**(2), 163–177 (1995)